# Observation of multiple types of topological fermions in PdBiSe

B. Q. Lv, Z.-L. Feng, J.-Z. Zhao, Noah F. Q. Yuan, A. Zong, K. F. Luo, R. Yu, Y.-B. Huang, V. N. Strocov, A. Chikina, A. A. Soluyanov, N. Gedik, Y.-G. Shi, T. Qian, and H. Ding

Phys. Rev. B **99**, 241104 — Published 7 June 2019

DOI: 10.1103/PhysRevB.99.241104

# Observation of multiple types of topological fermions in PdBiSe

B. Q. Lv,[1,2†] Z.-L. Feng,[1,3†] J.-Z. Zhao,[4,5†] Noah F. Q. Yuan,[2] A. Zong,[2] K. F. Luo,[6] R. Yu,[6] Y.-B. Huang,[7] V. N. Strocov,[8] A. Chikina,[8] A. A. Soluyanov,[9,10] N. Gedik,[2] Y.-G. Shi,[1*] T. Qian,[1,11*] H. Ding[1,11*]

[1] *Beijing National Laboratory for Condensed Matter Physics and Institute of Physics, Chinese Academy of Sciences, Beijing 100190, China*
[2] *Department of Physics, Massachusetts Institute of Technology, Cambridge, MA 02139, USA*
[3] *University of Chinese Academy of Sciences, Beijing 100049, China*
[4] *Co-Innovation Center for New Energetic Materials, Southwest University of Science and Technology*
[5] *Theoretical Physics and Station Q Zürich, ETH Zürich, 8093 Zürich, Switzerland*
[6] *School of Physics and Technology, Wuhan University, Wuhan 430072, China*
[7] *Shanghai Synchrotron Radiation Facility, Shanghai Institute of Applied Physics, Chinese Academy of Sciences, Shanghai 201204, China*
[8] *Paul Scherrer Institute, Swiss Light Source, CH-5232 Villigen PSI, Switzerland*
[9] *Physik-Institut, University of Zürich, Winterthurerstrasse 190, CH-8057 Zürich, Switzerland*
[10] *Department of Physics, St. Petersburg State University, St. Petersburg, 199034, Russia*
[11] *CAS Center for Excellence in Topological Quantum Computation, University of Chinese Academy of Sciences, Beijing 100190, China*

[†] These authors contributed to this work equally.

[*] Corresponding authors: dingh@iphy.ac.cn, tqian@iphy.ac.cn, ygshi@iphy.ac.cn

## Abstract

**Topological semimetals with different types of band crossings provide a rich platform to realize novel fermionic excitations, known as topological fermions. In particular, some fermionic excitations can be direct analogues of elementary particles in quantum field theory when both obey the same laws of physics in the low-energy limit. Examples include Dirac and Weyl fermions, whose solid-state realizations have provided new insights into long-sought phenomena in high-energy physics. Recently, theorists predicted new types of fermionic excitations in condensed-matter systems without any high-energy counterpart, and their existence is protected by crystalline symmetries. By studying the topology of the electronic structure in PdBiSe using density functional theory calculations and bulk-sensitive soft X-ray angle-resolved photoemission spectroscopy, we demonstrate a coexistence of four different types of topological fermions: Weyl, Rarita-Schwinger-Weyl, double class-II three-component, and charge-2 fourfold fermions. Our discovery provides a remarkable platform to realize multiple novel fermions in a single solid, charting the way forward to studies of their potentially exotic properties as well as their interplay.**

Topological semimetals are characterized by symmetry-protected band crossings, which may give rise to quasi-particle excitations and topological features that underlie exotic transport and optical properties [1]. The most famous examples are Dirac [Fig. 1(a)(iii)] [2-9] and Weyl semimetals [Fig. 1(a)(i)] [10-18]. They have been realized in various compounds in condensed-matter physics [2-18], which provides an alternative and simple platform to study the novel physics of elementary particles, especially the long-sought Weyl fermions, in high-energy physics. Only three types of fermions are allowed in high-energy physics – Dirac, Weyl, and Majorana fermions, while the zoology of topological fermions in semimetals is much richer. This is because low-energy excitations in topological semimetals are constrained by the space group symmetries of the crystal, which are usually much lower than the Poincaré symmetry imposed by the quantum field theory. Indeed, various types of semimetals with topological fermions have been proposed in the past few years [2-4,10-14,21-30], which can be briefly classified by the degeneracy and topological charge of band-crossing points in the momentum space [Fig. 1(a)]. Panel (i) shows three types of Weyl fermions with twofold degeneracy. In type-I Weyl semimetals, the Weyl points arise from two linear dispersions with opposite Fermi velocities along all momentum directions, whereas in type-II Weyl semimetals Fermi velocities share the same sign along a certain direction [14]. Besides the type-I and type-II fermions with $C = \pm 1$, theorists predicted another type of Weyl fermion, quadratic Weyl fermion with $C = \pm 2$, which is formed by two quadratic bands [11]. Panel (ii) shows symmetry-protected crossings with threefold degeneracy, giving rise to two classes of unconventional three-component fermions: class-I is characterized by one non-degenerate and one doubly-degenerate linear band crossings at separate points, which carry no topological charge [25-27,31,32]; class-II is formed by three non-degenerate bands with $C = \pm 2$ [23]. Moving on to fourfold band degeneracy in panel (iii), besides the well-known Dirac fermions, we note two types of unconventional fermions differentiated by their topological charges: charge-2 fourfold fermions ($C = \pm 2$) and Rarita-Schwinger-Weyl fermions ($C = \pm 4$) [29]. For even higher band degeneracies, shown in panels (iv) and (v), theory predicted double class-II three-component fermions ($C = \pm 4$) and double Dirac fermions ($C = 0$) [22,23], which can be viewed as a nontrivial doubling of class-II three-component fermions and Dirac fermions, respectively. Despite many proposals of material candidates for hosting these unconventional topological fermions [21-30], experimental evidence has been scant.

In this Letter, we expand the experimental horizon by simultaneously observing four different types of symmetry-stabilized topological fermions in a single solid-state system, PdBiSe. Using angle-resolved photoemission spectroscopy (ARPES) operating at the soft X-ray energy, we identified the coexistence of Weyl, Rarita-Schwinger-Weyl, double class-II three-component, and charge-2 fourfold fermions at different time-reversal invariant momenta of PdBiSe, all matching our expectation from density functional theory (DFT) calculations.

High-quality single crystals of PdBiSe were grown by the self-flux method. Soft X-ray ARPES measurements were performed at the Advanced Resonant Spectroscopies (ADRESS) beamline at the Swiss Light Source (SLS) [33], and at the 'Dreamline' beamline of the Shanghai Synchrotron Radiation Facility (SSRF). The DFT calculations were performed using the Vienna *ab-initio* simulation package (VASP) [34-38]. For details, see the Supplemental Material I [39].

PdBiSe has a noncentrosymmetric structure [Fig. 1(b)] with space group $P2_13$

(No. 198). The crystal is cubic and chiral, lacking inversion and mirror symmetries. Despite the cubic unit cell, the fourfold rotational symmetry is broken due to the chiral structure. Two important symmetries remaining are the threefold rotation symmetry ($C_3$) along the (111) axis and the twofold screw symmetry along the $z$ and $x$-axis. The calculated electronic band structure in the absence of spin-orbit coupling (SOC) is shown in Fig. 1(d). Without considering the spin degree of freedom, at the Γ point, a band crossing with threefold degeneracy is observed at ~ 0.7 eV below the Fermi level ($E_F$), which is protected by the $C_3$ symmetry. Its low-energy quasiparticle excitations can be described by a class-II three-component fermion shown in Fig. 1(a)(ii), whose crossing point is a monopole possessing a topological charge of + 2. On the other hand, at the R point, the bulk bands feature a fourfold degenerate band crossing below $E_F$, which is a charge-2 fourfold fermion with $C = -2$.

With the inclusion of SOC [Fig. 1(e)], due to a lack of inversion symmetry, the bands split at all momenta, commonly known as a Rashba-type band splitting. There are two exceptions in the momentum space where degeneracy remains: (i) time reversal invariant momenta, where Kramers theorem guarantees the double degeneracy, and (ii) Brillouin zone boundaries (X-M and M-R), where the screw symmetry ensures the double degeneracy as well. At certain time-reversal invariant momenta, the bulk bands have different types of symmetry-enforced crossings near $E_F$, which we identify with various topological fermions from detailed DFT calculations. First, at the Γ point, the crossings are either twofold or fourfold degenerate [Figs. 1(e) and 1(f)], corresponding to a Weyl fermion and a Rarita-Schwinger-Weyl fermion with $C = +4$. Second, at the R point, there is a band crossing with sixfold degeneracy [Figs. 1(e) and 1(g)], which is a double class-II three-component fermion with $C = -4$. Third, the bulk bands at the M point have fourfold degenerate points at ~ 1.1 eV below $E_F$ and ~ 0.15 eV above $E_F$, which are charge-2 fourfold fermions with $C = +2$. Lastly, PdBiSe also hosts type-I and type-II Weyl fermions at the X point and along the Γ-X, Γ- R directions [Figs. 1(e), 1(f), and 1(h)], respectively. To further illustrate the multifold band degeneracies at the Γ and R points, effective Hamiltonians at each point are constructed, giving the correct degeneracy as observed in the experiment (Supplemental Material II [39]).

To test the predictions by our calculations, we first perform core-level photoemission and X-ray diffraction measurements to confirm the chemical composition and the (001) surface orientation of PdBiSe (Supplemental Material I [39]). Next, we systematically investigate the bulk electronic structure using soft X-ray ARPES measurements on the (001) surface. The high energy of soft X-ray leads to a long escape depth of photoelectrons compared to vacuum ultraviolet (VUV) sources, significantly improving the bulk sensitivity as well as the $k_z$ resolution of the measurement [40]. Note that we also performed surface sensitive VUV ARPES measurements on the (001) surface, on which we successfully resolved the Dirac surface states (Supplemental Material IV [39]). Figure 2 displays the Fermi surfaces in three different high-symmetry planes. The measured Fermi surfaces in the vertical Γ-M-X-R plane (FS1) exhibit a modulation along the $k_z$ direction with a period of $2\pi/c$ [Fig. 2(b)], where $c$ is the lattice constant, confirming the bulk nature of the detected spectra. The Fermi surfaces at $k_z = 0$ (FS2) and $k_z = \pi$ (FS3) exhibit ring-like features centered at the Γ point [Fig. 2(d)] and the M point [Fig. 2(f)], or rhombic pockets surrounding the R point [Fig. 2(f)], which are in good agreement with calculations [Figs. 2(e) and 2(g)]. Note that the splitting of Fermi surfaces is not resolved in Figs. 2(b), 2(d), and 2(f) under current momentum and energy resolution, however, the band splitting can be resolved by high-precision measurements of the band dispersions, as we discuss later.

In the following, we demonstrate the signatures of different topological fermions in PdBiSe by using high-precision measurements of the band dispersions. We start by showing the topological fermions at the Γ point. The ARPES intensity and corresponding curvature plots [41] in Figs. 3(a) and 3(b) show a crossing point at ~ 0.85 eV below $E_F$, which matches our theoretical prediction of a Rarita-Schwinger-Weyl point protected by the $C_3$ rotational symmetry [Fig. 3(c)]. From the calculation, this crossing is fourfold degenerate, resulting from four electron-like bands along the Γ–X direction, labeled 1 to 4 in Fig. 3(c). As there is no inversion symmetry, the four bands are no longer degenerate away from the Γ or the X point, though the splitting is only significant between bands 1 and 2. This Rashba-type splitting is clearly observed in Figs. 3(a) and 3(b) (orange arrows). At the Γ point, we further observe an electron-like band whose bottom is at ~ 0.7 eV below $E_F$. Based on the calculation in Fig. 3(c), this bottom corresponds to a Weyl point protected by the Kramers theorem. Furthermore, our DFT calculations have identified multiple Weyl points at the X point [Fig. 1(h)]. Experimentally, it is very challenging to resolve these Weyl points by soft X-ray ARPES measurements, as they only differ by ~ 10 meV in energy. Though the fine features of these Weyl points are not resolved, the corresponding Weyl bands nearby are resolved in our measurements [Figs. 3(a) and 3(b)]. The observed ARPES spectra match well with the DFT calculations [Fig. 3(c)] and hence suggest the existence of multiple Weyl points at the X point.

Next, we reveal the evidence of a double class-II three-component fermion with sixfold band degeneracy at the R point. To visualize the degenerate crossing, we map out the band dispersions along the M-R direction with two photon energies that correspond to $k_z$ = 27π and 29π [Figs. 3(d) and 3(e)]. The measured electronic structure exhibits four doubly-degenerate bands around the R point, labeled 1 to 4 in Fig. 3(e). Among them, bands 1 to 3 are degenerate at R, forming a sixfold degenerate crossing, fully consistent with the theoretical calculations [Fig. 3(f)]. Note that besides the curvature intensity plot (Fig. 3(e)), the four bands can also be unambiguously resolved from the momentum distribution curve plot (Supplemental Material III [39]).

Last, to show the existence of charge-2 fourfold fermions at M point, we examine the M-X dispersion along the Brillouin zone boundary [Figs. 3(g)-3(i)]. Due to the screw symmetry, each band in this direction is twofold degenerate. In Figs. 3(g) and 3(h), we resolve two doubly degenerate dispersions, which meet at the M point at ~ 1.1 eV below $E_F$. The observed bands closely follow the calculated structure [Fig. 3(i)], demonstrating the existence of a charge-2 fourfold fermion at the M point.

One hallmark of topological fermions in solids is the existence of surface Fermi arcs connecting the projection of monopoles with opposite topological charges. For example, the surface Fermi arcs connecting the projection of Weyl points in TaAs is clearly resolved [15]. However, the monopoles do not necessarily guarantee the existence of observable surface Fermi arcs [28]. More specifically, if there is no gap in the vicinity of the projected bulk degenerate point (e.g., Weyl point) at a given surface, Fermi arcs cannot be observed (Supplemental Material IV [39]). The arguments above are manifested in PdBiSe. This is because the observed multiple band crossings in PdBiSe arise from Rashba-type splitting of the bulk bands, which are highly tilted and eventually disperse in the same directions away from these monopoles. Consequently, when these Rashba bulk bands are projected onto a given surface (e.g., the (001) surface), they will fill in all of the surface gaps in the vicinity of the projected monopoles, and obscure the associated topological Fermi arcs. Indeed, our slab calculations and surface sensitive VUV ARPES measurements confirmed the absence of the associated Fermi arc surface states on the (001) top surface [Fig. 1(b)] of PdBiSe. Instead, we identified several surface Dirac points at the time-reversal invariant momenta. Hence, PdBiSe also provides a remarkable platform to study the two-dimensional Dirac fermions (Supplemental Material IV [39]).

In contrast to the previous well studied Dirac and Weyl fermion systems which are driven by band inversion based on specific material parameters such as lattice constants and strength of SOC, the observed topological fermions in the present work are stabilized by the crystal symmetry and are therefore universal feature of a chiral crystal with space group $P2_13$ (No. 198). In this aspect, our work would open new possibilities to realize various types of topological fermions in many more material candidates with similar symmetry properties. We further note that PdBiSe is a non-centrosymmetric superconductor [42,43]. Hence, its split Fermi surfaces near $E_F$ could host rare coexistence of spin-singlet and spin-triplet superconducting pairing states (Supplemental Material V [39]).

In summary, by using DFT calculations and bulk-sensitive soft X-ray ARPES, we predicted and proved the coexistence of four different types of topological fermions in the electronic structure of PdBiSe. We identified twofold Weyl fermions ($C = \pm 1$) at the Γ and X point, fourfold Rarita-Schwinger-Weyl fermion ($C = +4$) at the Γ point, sixfold double class-II three-component fermion ($C = -4$) at the R point, and charge-2 fourfold fermion ($C = +2$) at the M point. These multiple topological fermions, which could couple through Coulomb interactions, are stabilized at different time-reversal invariant momenta by crystalline symmetries. Our observation thus paves the way for investigating novel physics related to these unconventional fermions as well as their interplay in a single condensed-matter system.

*Note added:* After completing the manuscript, we became aware of several related works posted on arXiv:1809.01312 [44], arXiv:1901.03358 [45], arXiv:1812.04466 [46] and arXiv:1812.03310 [47], showing the realization of unconventional fermions in solids. More specifically, Refs. 44, 45, and 46 reported the observation of topological fermions with monopole charges of ± 2 in Co(Rh)Si, and Ref. 47 discussed topological fermions with monopole charges of ± 4 in AlPt. In the present work, PdBiSe represents a richer platform with the coexistence of four different types of topological fermions, i.e., Weyl ($C = \pm 1$), Rarita-Schwinger-Weyl ($C = +4$), double class-II three-component ($C = -4$), and charge-2 fourfold fermions ($C = +2$). More importantly, PdBiSe is one of the first systems where fermions with monopole charges of ± 4 are experimentally identified. These fermions are topologically distinct from those in Co(Rh)Si.

## References


[1] N. P. Armitage, E. J. Mele, and A. Vishwanath, Rev. Mod. Phys. **90**, 015001 (2018).

[2] Z. Wang, Y. Sun, X.-Q. Chen, C. Franchini, G. Xu, H. Weng, X. Dai, and Z. Fang, Phys. Rev. B **85**, 195320 (2012).

[3] S. M. Young, S. Zaheer, J. C. Y. Teo, C. L. Kane, E. J. Mele, and A. M. Rappe, Phys. Rev. Lett. **108**, 140405 (2012).

[4] Z. Wang, H. Weng, Q. Wu, X. Dai, Z. Fang, Phys. Rev. B **88**, 125427 (2013).

[5] Z. K. Liu, J. Jiang, B. Zhou, Z. J. Wang, Y. Zhang, H. M. Weng, D. Prabhakaran, S.-K. Mo, H. Peng, P. Dudin, T. Kim, M. Hoesch, Z. Fang, X. Dai, Z. X. Shen, D. L. Feng, Z. Hussain, and Y. L. Chen, Science **343**, 864–867 (2014).

[6] S. Borisenko, Q. Gibson, D. Evtushinsky, V. Zabolotnyy, B. Bu□chner, and R. J. Cava, Phys. Rev. Lett. **113**, 027603 (2014).

[7] M. Neupane, S. –Y. Xu, R. Sankar, N. Alidoust, G. Bian, C. Liu, I. Belopolski, T. –R. Chang, H. –T. Jeng, H. Lin, A. Bansil, F. Chou, and M. Z. Hasan, Nat. Commun. **5**, 3786 (2014).

[8] Z. K. Liu, B. Zhou, Y. Zhang, Z. J. Wang, H. M. Weng, D. Prabhakaran, S.-K. Mo, Z. X. Shen, Z. Fang, X. Dai, Z. Hussain, and Y. L. Chen, Nature Mater. **13**, 677–681 (2014).

[9] S.-Y. Xu, C. Liu, S. K. Kushwaha, R. Sankar, J.W. Krizan, I. Belopolski, M. Neupane, G. Bian, N. Alidoust, T.-R.Chang, H.-T. Jeng, C.-Y. Huang, W.-F. Tsai, H. Lin, P. P. Shibayev, F.-C. Chou, R. J. Cava, and M. Z. Hasan, Science **347**, 294 (2015).

[10] X. Wan, A. M. Turner, A. Vishwanath, and S. Y. Savrasov, Phys. Rev. B **83**, 205101 (2011).

[11] G. Xu, H. Weng, Z. Wang, X. Dai, and Z. Fang, Phys. Rev. Lett.**107**, 186806 (2011).

[12] H. Weng, C. Fang, Z. Fang, B. A. Bernevig, and X. Dai, Phys. Rev. X **5**, 011029 (2015).

[13] S.-M. Huang, S.-Y. Xu, I. Belopolski, C.-C. Lee, G. Chang, B. Wang, N. Alidoust, G. Bian, M. Neupane, C. Zhang, S.Jia, A. Bansil, H. Lin, and M. Z. Hasan, Nat. Commun. **6**, 7373 (2015).

[14] A. A. Soluyanov, D. Gresch, Z.Wang, Q. Wu, M. Troyer, X. Dai, and B. A. Bernevig, Nature **527**, 495–498 (2015).

[15] B. Q. Lv, H. M. Weng, B. B. Fu, X. P. Wang, H. Miao, J. Ma, P. Richard, X. C. Huang, L. X. Zhao, G. F. Chen, Z. Fang, X. Dai, T. Qian, and H. Ding, Phys. Rev. X **5**, 031013 (2015).

[16] S.-Y. Xu, I. Belopolski, N. Alidoust, M. Neupane, G. Bian, C. Zhang, R. Sankar, G. Chang, Z. Yuan, C.-C. Lee, S.-M. Huang, H. Zheng, J. Ma, D. S. Sanchez, B.Wang, A. Bansil, F. Chou, P. P. Shibayev, H. Lin, S. Jia, and M. Z. Hasan, Science **349**, 613–617 (2015).

[17] B. Q. Lv, N. Xu, H. M. Weng, J. Z. Ma, P. Richard, X. C. Huang, L. X. Zhao, G. F. Chen, C. E. Matt, F. Bisti, V. N. Strocov, J. Mesot, Z. Fang, X. Dai, T. Qian, M. Shi, and H. Ding, Nature Phys. **11**, 724-727 (2015).

[18] L. X. Yang, Z. K. Liu, Y. Sun, H. Peng, H. F. Yang, T. Zhang, B. Zhou, Y. Zhang, Y. F. Guo, M. Rahn, D. Prabhakaran, Z. Hussain, S.-K. Mo, C. Felser, B. Yan, and Y. L. Chen, Nature Phys. **11**, 728-732 (2015).

[19] P.A. M. Dirac, Proc. R. Soc. A **117**, 610–24(1928).

[20] H. Weyl, Z. Phys. **56**, 330 (1929).
[21] T. T. Heikkilä, and G. E. Volovik, New J. Phys. **17,** 093019 (2015).
[22] B. J. Wieder, Y. Kim, A. M. Rappe, and C. L. Kane, Phys. Rev. Lett. **116**, 186402 (2016).
[23] B. Bradlyn, J. Cano, Z. Wang, M. G. Vergniory, C. Felser, R. J. Cava, and B. A. Bernevig, Science **353**, aaf5037 (2016).
[24] T. Hyart, and T. T. Heikkilä. Phys. Rev. B **93**, 235147 (2016).
[25] H. Weng, C. Fang, Z. Fang, and X. Dai. Phys. Rev. B **93**, 241202(R) (2016).
[26] H. Weng, C. Fang, Z. Fang, and X. Dai. Phys. Rev. B **94**, 165201 (2016).
[27] Z. Zhu, G. W. Winkler, Q. S. Wu, J. Li, and A. A. Soluyanov, Phys. Rev. X **6**, 031003 (2016).
[28] G. Chang, S-Y. Xu, B. J. Wieder, D. S. Sanchez, S.-M. Huang, I. Belopolski, T.-R. Chang, S. Zhang, A. Bansil, H. Lin, and M. Z. Hasan, Phys. Rev. Lett. **119**, 206401 (2017).
[29] P. Tang, Q. Zhou, and S. C. Zhang, Phys. Rev. Lett. **119**, 206402 (2017).
[30] T. Zhang, Z. Song, A. Alexandradinata, H. Weng, C. Fang, L. Lu, and Z. Fang, Phys. Rev. Lett. **120**, 016401 (2018).
[31] B. Q. Lv, Z.-L. Feng, Q.-N. Xu, X. Gao, J.-Z. Ma, L.-Y. Kong, P. Richard, Y.-B. Huang, V. N. Strocov, C. Fang, H.-M.Weng, Y.-G. Shi, T. Qian, and H. Ding, Nature **546**, 627-631 (2017).
[32] J.-Z. Ma, J.-B. He, Y.-F. Xu, B.-Q. Lv, D. Chen, W.-L. Zhu, S. Zhang, L.-Y. Kong, X. Gao, L.-Y. Rong, Y.-B. Huang, P. Richard, C.-Y. Xi, Y. Shao, Y.-L. Wang, H.-J.Gao, X. Dai, C. Fang, H.-M. Weng, G.-F.Chen, T. Qian, and H. Ding, Nat. Phys. **14**, 349–354 (2018).
[33] V. N. Strocov, X. Wang, M. Shi, M. Kobayashi, J. Krempasky, C. Hess, T. Schmitt, and L. Patthey, J. Synchrotron Radiat. **21**, 32–44 (2014).
[34] P. E. Blochl, Phys. Rev. B **50**, 17953 (1994).
[35] J. P. Perdew, K. Burke, and M. Ernzerhof, Phys. Rev. Lett. **77**, 3865 (1996).
[36] G. Kresse, and J. Hafner, Phys. Rev. B **48**, 13115 (1993).
[37] G. Kresse, and J. Furthmuller, Phys. Rev. B **54**, 11169 (1996).
[38] G. Kresse, and D. Joubert, Phys. Rev. B **59**, 1758 (1999).
[39] See supplemental materials for more details.
[40] V. N. Strocov, M. Shi, M. Kobayashi, C. Monney, X. Wang, J. Krempasky, T. Schmitt, L. Patthey, H. Berger, and P. Blaha, Phys. Rev. Lett. **109**, 086401 (2012).
[41] P. Zhang, P. Richard, T. Qian, Y.-M. Xu, X. Dai, and H. Ding, Rev. Sci. Instrum. **82**, 43712 (2011).
[42] B. Joshi, A. Thamizhavel, and S. Ramakrishnan, J. Phys.: Conf. Ser. **592** 012069 (2015).
[43] M. Kakihana, A. Nakamura, A. Teruya, H. Harima, Y. Haga, M. Hedo, T. Nakama, and Y. Onuki, J. Phys. Soc. Jpn. **84**, 033701 (2015).
[44] D. Takane, Z. Wang, S. Souma, K. Nakayama, T. Nakamura, H. Oinuma, Y. Nakata, H. Iwasawa, C. Cacho, T. Kim, K. Horiba, H. Kumigashira, T. Takahashi, Y. Ando, and T. Sato, Phys. Rev. Lett. **122**, 076402 (2019).
[45] Z. -C. Rao, H. Li, T. Zhang, S. Tian, C. Li, B. Fu, C. Tang, L. Wang, Z. Li, W. Fan, J. Li, Y. Huang, Z. Liu, Y. Long, C. Fang, H. Weng, Y. Shi, H. Lei, Y. Sun, T. Qian, and H. Ding, Nature **567**, 496-499 (2019).
[46] D. S. Sanchez, I. Belopolski, T. A. Cochran, X. Xu, J. –X. Yin, G. Chang, W. Xie, K. Manna, V. Su□ß, C. –Y. Huang, N. Alidoust, D. Multer, S. S. Zhang, N.

Shumiya, X. Wang, G. –Q. Wang, T. –R. Chang, C. Felser, S. –Y. Xu, S. Jia, H. Lin, and M. Z. Hasan, Nature **567**, 500-505 (2019).

[47] N. B. M. Schröter, D. Pei, M. G. Vergniory, Y. Sun, K. Manna, F. Juan, J. A. Krieger, V. Su□ss, M. Schmidt, P. Dudin, B. Bradlyn, T. K. Kim, T. Schmitt, C. Cacho, C. Felser, V. N. Strocov, and Y. Chen, Nature Physics (2019). DOI: 10.1038/s41567-019-0511-y

## Acknowledgements

This work was supported by the Ministry of Science and Technology of China (2016YFA0401000, 2016YFA0300600, 2015CB921300, and 2017YFA0302901), the Chinese Academy of Sciences (XDB28000000, XDB07000000, and QYZDB-SSW-SLH043), the National Natural Science Foundation of China (11622435, U1832202, 11474340, 11474330, 11604273, and 11774399), and the Beijing Municipal Science and Technology Commission (No. Z171100002017018). N.G., B.Q.L. and A.Z. acknowledge support from the National Science Foundation under Grant No. NSF DMR-1809815 (data analysis), and the Gordon and Betty Moore Foundation's EPiQS Initiative grant GBMF4540 (manuscript writing). J.Z.Z. was also supported by the Longshan academic talent research-supporting program of SWUST (17LZX527), and ETH Zurich for funding his visit, A.A.S. acknowledges the support of Swiss National Science Foundation (SNSF) Professorship, NCCR MARVEL and QSIT grants, as well as Microsoft Research. N F.Q.Y. is supported by the DOE Office of Basic Energy Sciences, Division of Materials Sciences and Engineering under award de-sc0010526. Y.B.H. acknowledges support from the CAS Pioneer "Hundred Talents Program" (type C). A.C. acknowledges funding from the Swiss National Science Foundation under the grant No. 200021_165529.

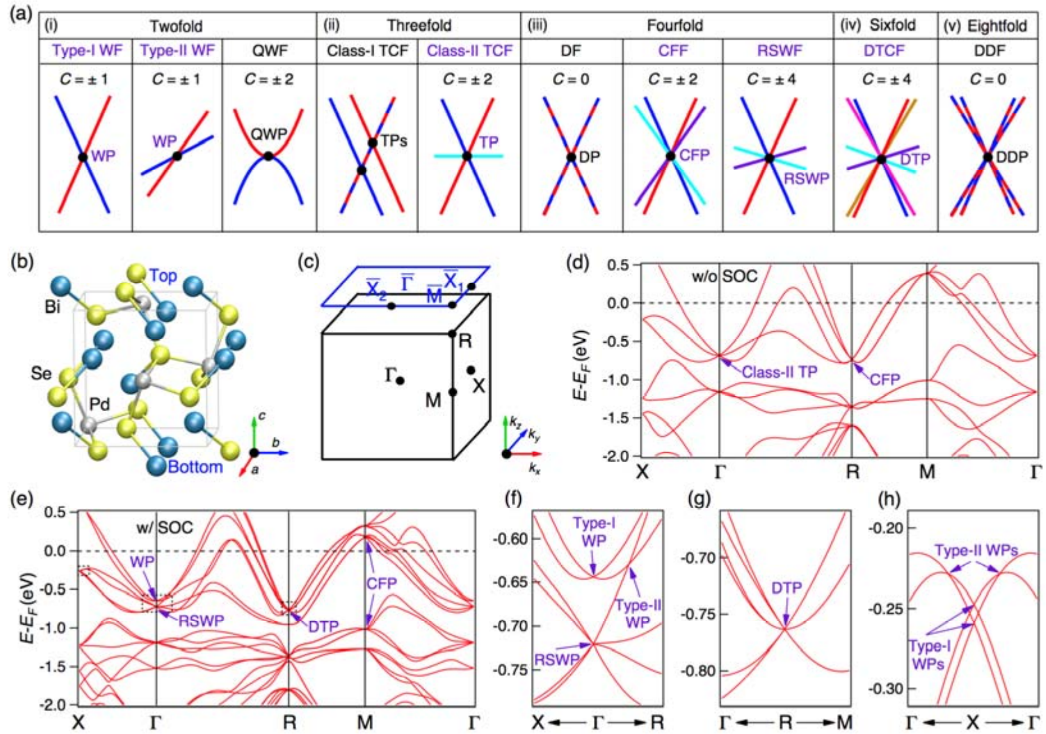


FIG. 1. (a) Schematic of the band structure of various topological fermions in condensed-matter systems. (b) Three-dimensional (3D) crystal structure of PdBiSe. (c) 3D bulk Brillouin zone (black) and the projected (001) surface Brillouin zone (blue), with high-symmetry points indicated. (d) and (e) Calculated band structures of PdBiSe along high-symmetry lines without (d) and with (e) spin-orbit coupling. The dashed boxes indicate the regions of interest shown in (f), (g), and (h), respectively. (f)-(h) Calculated fine band structures. WF/WP: Weyl fermion/point; QWF/QWP: quadratic Weyl fermion/point; TCF: three-component fermion, TP: triple point; DF/DP: Dirac fermion/point; CFF/CFP: charge-2 fourfold fermion/point; RSWF/RSWP: Rarita-Schwinger-Weyl fermion/point; DTCF: double class-II three-component fermion, DTP: double triple point; DDF/DDP: double Dirac fermion/point.

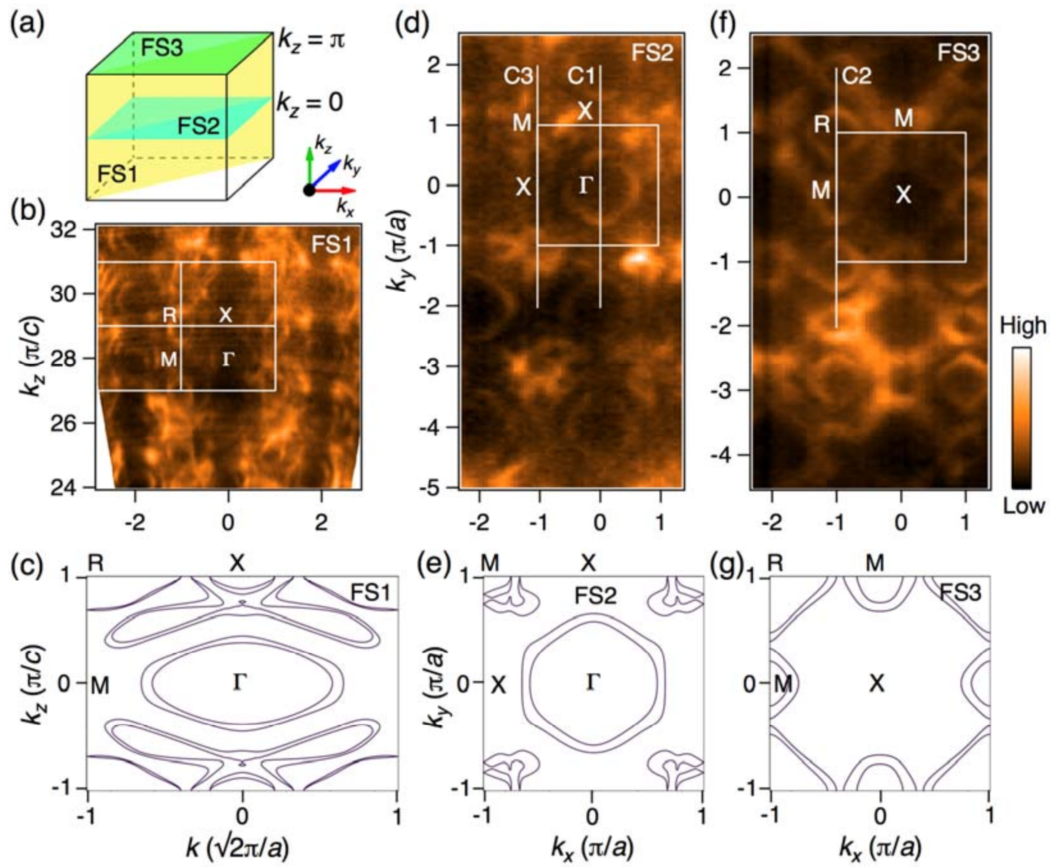


FIG. 2. (a) Bulk Brillouin zone with three high-symmetry planes, which indicate the locations of the measured Fermi surfaces in (b), (d), and (f) respectively. (b) and (c) Experimental (b) and calculated (c) intensity plots at $E_F$, showing the Fermi surface in the vertical Γ-M-X-R plane (FS1). The white boxes indicate the bulk Brillouin zone boundary. (d) and (e) Experimental (d) and calculated (e) intensity plots at $E_F$, showing Fermi surfaces in the $k_z$ = 0 plane (FS2). The white boxes indicate the Brillouin zone boundary in the $k_z$ = 0 plane. (f) and (g) The same as (d) and (e) but in the $k_z$ = π plane. The white lines C1, C2 and C3 in (d) and (f) indicate the momentum cuts in Fig. 3. All data were taken on the (001) surface at 20 K.

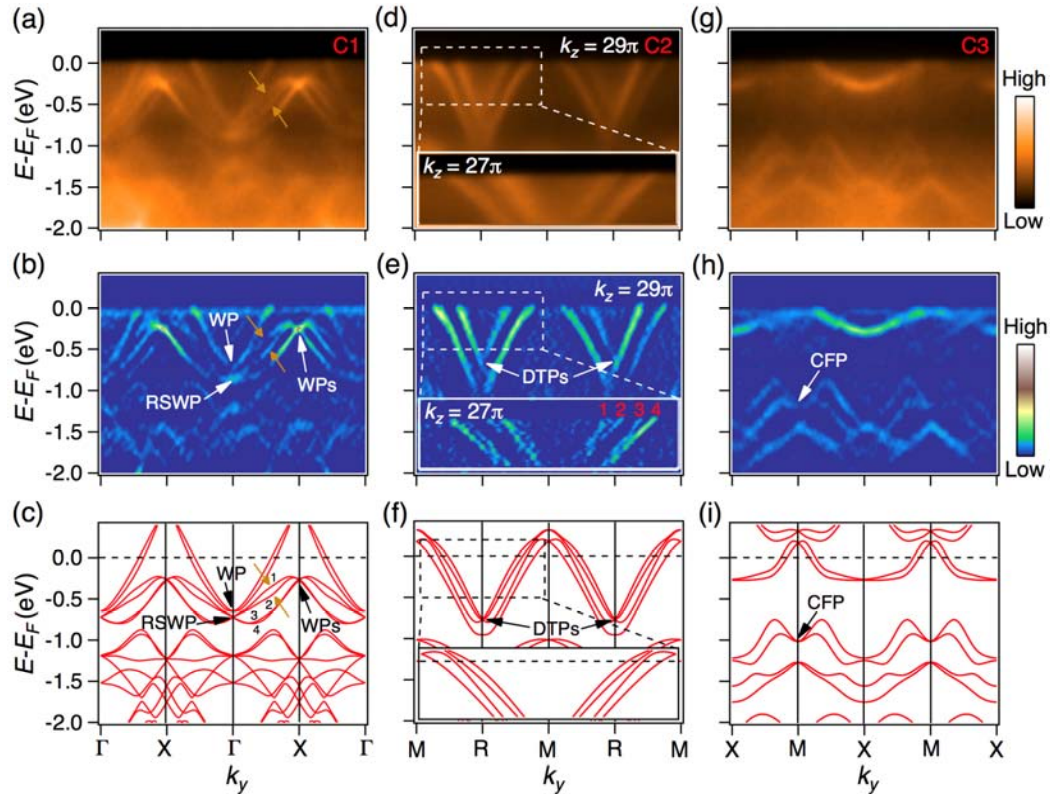


FIG. 3. (a)–(c) ARPES (a) and curvature (b) intensity plots and the calculated band structure (c) along C1 [white line in Fig. 2(d)]. Orange arrows indicate band splitting. (d)–(f) The same as (a)–(c) but along C2 [white line in Fig. 2(f)]. The insets in (d)-(f) show the enlarged image, and the normal and enlarged data in (d) and (e) were recorded with photon energy $h\nu$ = 745 eV ($k_z$ = 29π) and 550 eV ($k_z$ = 27π), respectively. (g)–(i) The same as (a)–(c) but along C3 [white line in Fig. 2(d)].